

Supplemental Information A. Error in mass balance calculations with δ -values

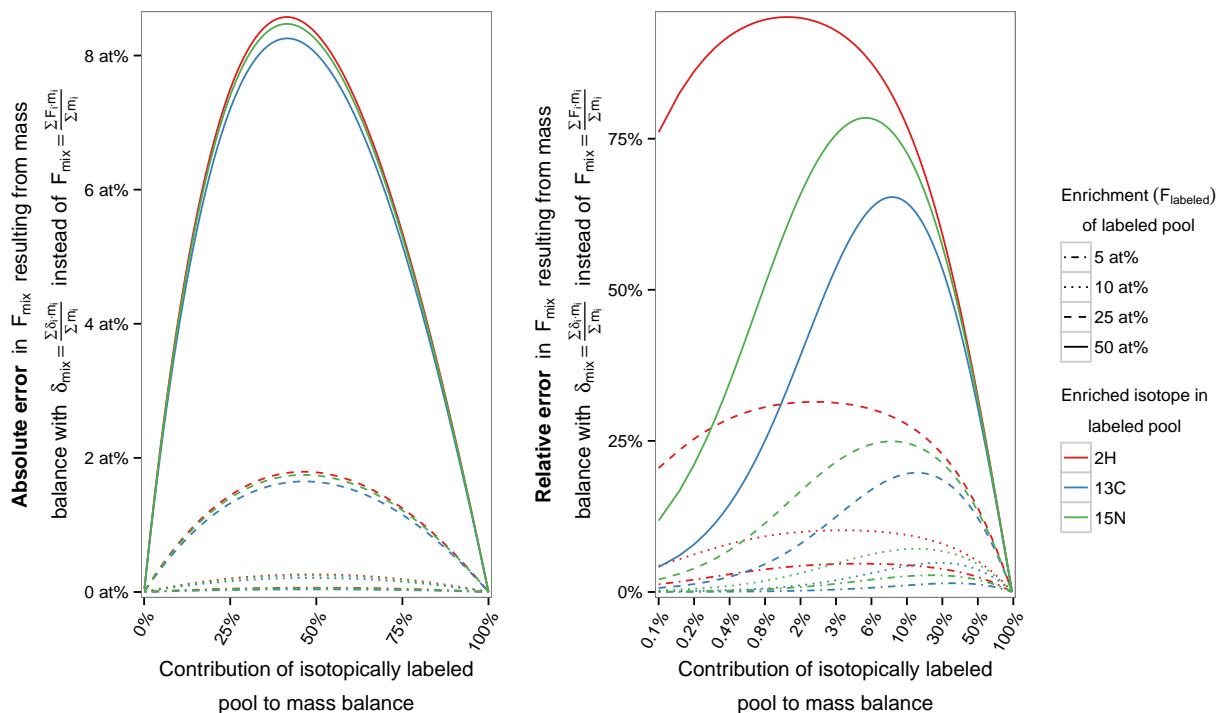


Figure A.6: **Errors in mass balance calculations with δ -values.** Absolute (left) and relative (right) error introduced by mass balance calculations using the δ -value approximation ($\delta_{mix} \sum m_i \approx \sum \delta_i m_i$) instead of fractional abundances ($F_{mix} \sum m_i = \sum F_i m_i$). Errors introduced by the approximation are illustrated for hydrogen, carbon and nitrogen and plotted as a function of mixing between an isotopically unlabeled (natural abundance) end-member and an isotopically enriched pool (ranging in fractional abundance of the rare isotope from 5 at% to 50 at%).

Isotopic mass balance can be approximated with isotopic values in δ -notation ($\delta_{mix} \sum m_i \approx \sum \delta_i m_i$) when the isotopic composition of all pools is relatively close to natural abundance. However, this approximation introduces significant error when one or multiple pools of heavily enriched materials are part of the mass balance. This is routinely the case when working with isotopic labels and it is important to use exact mass balance calculations with fractional abundance values F instead, i.e. $F_{mix} \sum m_i = \sum F_i m_i$. Figure A.6 illustrates the absolute and relative error introduced in the estimate of F_{mix} if mass balance between an isotopically labeled and a natural abundance (unlabeled) pool is calculated using δ -values (and then converted to F_{mix} for comparison) vs. the exact calculation in abundance space. Mass balance using δ -values systematically overestimates the true value. The error scales with the strength of the isotope label (here pictured up to a composition of $F_{labeled} = 50\%$ rare isotope in the labeled pool) and is slightly more pronounced for isotopic

systems with lower natural abundance isotope ratios (error for H > N > C). It is important to note that while the absolute error introduced from calculations with δ -values is most pronounced at a \sim 1:1 mixing ratio (slightly offset from 50% because natural abundances are not 0%), relative errors in the estimate for F_{mix} reach significant levels (> 10%) already with very little addition of a heavy isotope label. This aspect of δ -value mass balance limits the ability to accurately infer microbial activity in isotope labeling experiments. For this reason, fractional abundances were used for all mass balance calculations in this study.

Supplemental Information B. Error from shot noise

Even if detection, amplification and signal conversion in isotope ratio measurements were completely free of noise, there would still be a theoretical limit to the maximum attainable precision of isotopic data. This limit is posed by shot noise, a consequence of the discrete nature of electronic charge (whether it is carried by electrons or ions). The statistical error from shot noise is rarely a concern in standard bulk isotope measurements, but due to the low number of ions detected and limited chance for reanalysis from measuring individual cells in secondary ion mass spectrometry, this error estimate provides an important constraint on precision. This is particularly relevant in measurements of ions from low abundance elements, ions with low ionization efficiency or with rare minor isotopes (hydrogen qualifies for the last two). The error from shot noise is often considered in terms of the resulting isotope ratio or δ -value (Fitzsimons et al., 2000; Hayes, 2002), but rarely in terms of fractional abundances.

The number of ions N observed at a detector in a fixed time interval t follows a Poisson distribution (i.e., a discrete probability distribution of independent events occurring with an average rate of a). The corresponding probability mass function is $f(N) = P(X = N) = \frac{(at)^N e^{-at}}{N!}$. The expected value $E[N] = \bar{N}$ (mean) of a Poisson distribution is $\bar{N} = at$ (for a fixed time interval t). The variance $Var[N]$ of a Poisson distribution is identical to the expected value, and hence the standard deviation σ_N scales with the square root of \bar{N} ($\sigma_N = \sqrt{Var[N]} = \sqrt{\bar{N}}$). This has two important consequences for the quantification of ion currents in secondary ion mass spectrometry:

- The relative error $\frac{\sigma_N}{\bar{N}} = \frac{1}{\sqrt{\bar{N}}}$ decreases with higher ion counts (i.e. longer counting at constant rates makes the measurement more precise)
- There are diminishing returns due to the $\sqrt{\bar{N}}^{-1}$ dependence

As a concrete example, consider an ion current of 1000 ions/s. If you repeatedly observed this ion beam for exactly 1s, you would detect 1000 ions *on average*, but with $\sigma_N = 31.6$ (or 3.16% error). If you repeatedly observed this same ion beam for 2s instead, you would detect 2000 ions on average, but with $\sigma_N = 44.7$ (or 2.24% error, a $\sqrt{2}^{-1}$ improvement). This counting error ($\sigma_N = \sqrt{\bar{N}}$) is propagated readily to the resulting isotope ratios $R = \frac{i_m}{i_M}$ (m =minor, M =major isotope), fractional abundances $F = \frac{i_m}{i_M + i_m}$ and δ -values $\delta = \frac{R_1}{R_2} - 1$ by standard

error propagation. For details on σ_R and σ_δ , see Fitzsimons et al. (2000); Hayes (2001). σ_F is derived as follows:

$$\begin{aligned}
\sigma_F^2 &= \left(\frac{\partial F}{\partial N_m}\right)^2 \sigma_{N_m}^2 + \left(\frac{\partial F}{\partial N_M}\right)^2 \sigma_{N_M}^2 = \left(\frac{N_M}{(N_m + N_M)^2}\right)^2 \sigma_{N_m}^2 + \left(-\frac{N_m}{(N_m + N_M)^2}\right)^2 \sigma_{N_M}^2 \\
&= \frac{N_M^2 N_m^2}{(N_m + N_M)^4} \left[\left(\frac{\sigma_{N_m}}{N_m}\right)^2 + \left(\frac{\sigma_{N_M}}{N_M}\right)^2 \right] = F^2 (1 - F)^2 \left[\left(\frac{\sigma_{N_m}}{N_m}\right)^2 + \left(\frac{\sigma_{N_M}}{N_M}\right)^2 \right] \\
\rightarrow \left(\frac{\sigma_F}{F}\right)^2 &= (1 - F)^2 \left(\frac{1}{N_m} + \frac{1}{N_M} \right) = \frac{(1 - F)^2}{N_M F}
\end{aligned} \tag{B.1}$$

Supplemental Information C. Single cell analysis in plastic

Multi-isotope imaging mass spectrometry in thin section vastly expands the range of applicability of this technique to complex systems. However, many thin sectioning techniques with a relatively soft, removable matrix (e.g. embedding in OCT for cryosectioning, or embedding in paraffin) do not permit cutting sections thinner than $\sim 5\mu\text{m}$. While less problematic for large eukaryotic cells, this limits the potential applicability for microbial cells within larger communities or host systems where accurate targeting and identification of individual microbial cells in an ion image require even thinner sections. Hard polymerizing plastic resins developed for electron microscopy, such as LR White, provide the matrix support required for ultra-thin sections, however, they are often too dense to permit the easy use of fluorescent staining techniques important for microbial identification, such as fluorescence *in-situ* hybridization. Here, we thus use the plastic polymer Technovit, which is of intermediate hardness, and allows both routine sectioning to $\sim 1\mu\text{m}$ thickness as well as application of most fluorescent staining techniques (Takechi et al., 1999, McGlynn et al., in prep.). Technovit works well for preserving the structure of a sample and, unlike most resins, polymerizes at cold temperatures ($\sim 4^\circ\text{C}$), precluding the need for extended exposure to relatively high heat (and the associated risk for structural changes). The structural support lent by the plastic matrix provides thin sections with a smooth surface that enables high spatial resolution in imaging mass-spectrometry due to the lack of strong topological features. However, as an acryl plastic (a combination of methyl methacrylate and glycol methacrylate), the Technovit resin contributes significant amounts of isotopically circumnatural carbon and hydrogen that dilute the isotopic signal from enriched cells. It is thus imperative to calibrate and correct any isotopic measurements of single cells embedded in plastic.

To measure embedded bacterial isotope standards, aliquots of all standards were concentrated by centrifugation, suspended in a few drops of molten noble agar (2% Difco Agar Noble in 50mM HEPES buffered filter-sterilized water), solidified by cooling at room temperature, cut into $\sim 2\text{mm}^3$ cubes, resuspended in 50% EtOH in PBS, and dehydrated in 100% Ethanol over the course of 3 exchanges, with final resuspension in 100% for at least 1 hour. Ethanol was then replaced twice with 100% Technovit 8100 infiltration solution (Heraeus Kulzer GmbH, #64709012) to infiltrate the agar plugs over night. Agar plugs were finally suspended in airtight 0.6mL microcentrifuge tubes in Technovit 8100 infiltration solution amended with hardener II reagent and stored at 4°C

over night to complete polymerization. Technovit is a cold-polymerizing nitrogen-free acryl plastic composed of methyl methacrylate and glycol methacrylate.

Thin sections (1-2 μm thick) were cut using a rotary microtome. Each section was stretched on the surface of a 1.5 μL drop of 0.2 μm filtered deionized water on a 1" diameter round microprobe slides (Lakeside city, IL) and air-dried at room temperature. The glass rounds were mapped microscopically with a 40x air objective for later orientation and sample identification during secondary ion mass spectrometry. The rounds were sputter-coated with a 50nm layer of gold to provide a conductive surface (Dekas et al., 2009; Dekas and Orphan, 2011). Bacterial cells in the plastic sections were analyzed by NanoSIMS using a $\sim 1.9\text{pA}$ primary Cs^+ beam and were pre-sputtered with a $\sim 175\text{pA}$ primary Cs^+ beam current (I_{pre}) for 4 to 8 minutes (t), depending on the size of the pre-sputtering area (A), to a cumulative charge density of $\sim 350\text{pC}/\mu\text{m}^2$ ($I_{pre} \cdot t/A$).

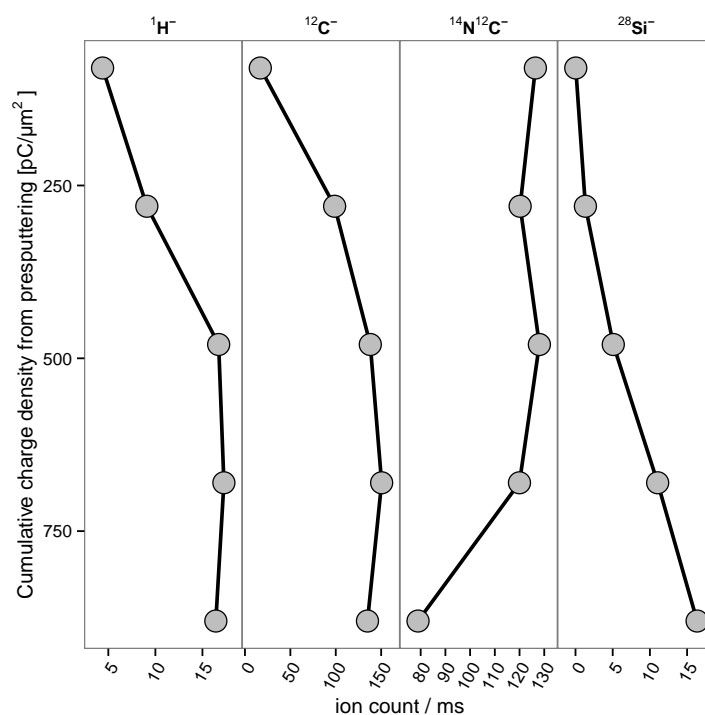


Figure C.7: **Ionization efficiency and sample ablation in embedded cells.** Ion counts of the major H, C and N ions, as well as Si after various extents of primary ion beam exposure (quantified as cumulative charge density $I_{pre} \cdot t/A$ from pre-sputtering with primary Cs^+ beam current $I_{pre} \approx 175 \text{ pA}$). Detection of $^{28}\text{Si}^-$ illustrates the gradual degradation of the plastic thin section to the point where the underlying glass support contributes increasingly to the secondary ion beam.

Figure C.7 illustrates the change in ion counts per ms for the major isotopes' ions as a function of pre-exposing plastic-embedded cells to increasing amounts of charge from the primary ion beam. Compared to whole single cells, the plastic matrix provides a material that is much more resilient to ion bombardment, as evidenced by the significantly higher pre-sputtering flux ($>10\times$ higher) required for an increase in ionization efficiency and sample

degradation. This is partly due to the gold coating, but the primary ion beam vaporizes the thin gold layer quickly (the gold is removed by the time of the first data point in Figure C.7), and is mostly a consequence of the plastic matrix. This figure also shows the same trends observed for whole cell analysis, namely the faster increase in ionization efficiency and subsequent quicker depletion of nitrogen. Additionally, $^{28}\text{Si}^-$ ions were collected in addition to H, C and N ions, and illustrate the gradual degradation of the plastic to the point where the underlying glass starts to contribute to the secondary ion beam.

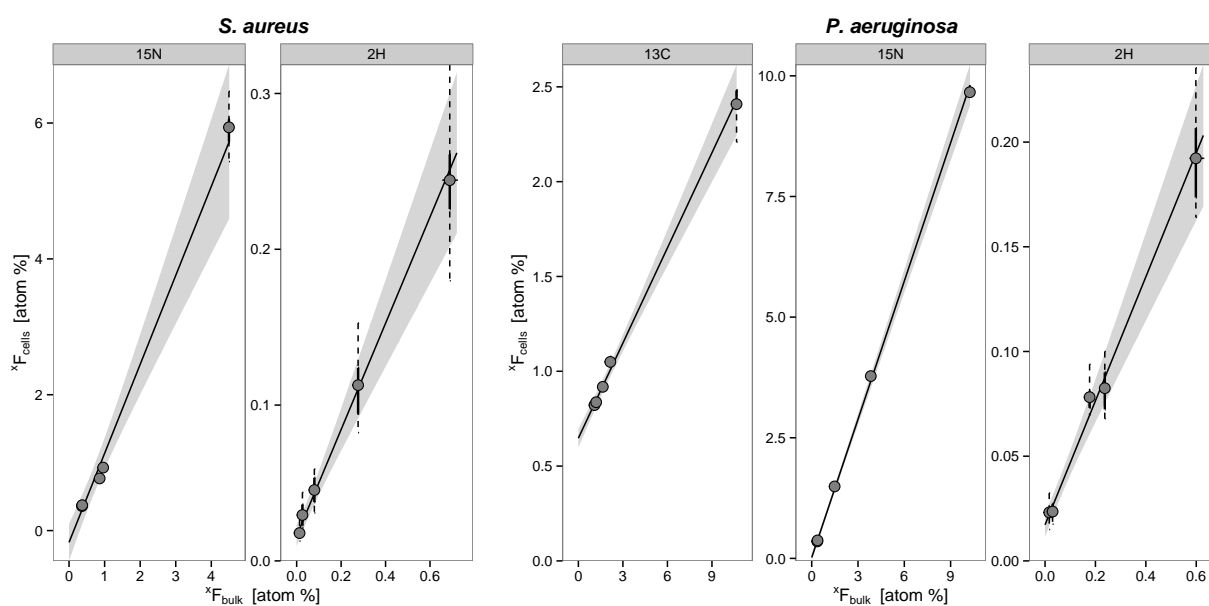


Figure C.8: **Calibration curves for single cell vs. bulk isotope analysis.** Isotopic composition of bacterial isotope standards in embedded single cell analysis by NanoSIMS (119 ROIs for *P. aeruginosa* and 135 ROIs for *S. aureus*) vs. bulk analysis by EA-ir-MS (bulk ^{13}C and ^{15}N) and GC-pyrolysis-ir-MS (bulk fatty acid ^2H). All data are reported in fractional abundances $^x F$ (with $x = ^{13}\text{C}$, ^{15}N and ^2H). Data points represent the mean isotopic composition of all measured single cells. The solid vertical error bars for each data point represent the range that comprises 50% of the single cell data. The dashed vertical whiskers represent the entire range of all single cell measurements. Horizontal error bars represent the total range of measured bulk isotopic composition (smaller than symbol sizes in most cases). Linear regressions are shown with 95% confidence bands.

Figure C.8 shows the calibration curves for cells of *S. aureus* (based on 104 ROIs) and *P. aeruginosa* (based on 100 ROIs) embedded in Technovit. Table 1 provides details on all resulting calibration parameters. As expected, the nitrogen isotope compositions of embedded single cells for both organisms are not diluted by the plastic polymer (which contains no nitrogen). In *P. aeruginosa*, the calibration slope for embedded cells closely matches the slope for free whole cells (0.94 ± 0.06 and 0.95 ± 0.04), with near perfect linear correlation and slope close to 1. In the case of *S. aureus*, variability in the nitrogen isotopic composition of individual cells leads to large uncertainty observed in the calibration slope for embedded cells, which increases to 1.31 ± 0.29 and should be applied with caution.

Organism	Isotope	Calibration range (${}^x F_{bulk}$ [at%])	${}^x F_{cells}$ vs. ${}^x F_{bulk}$ slope	${}^x F_{cells}$ vs. ${}^x F_{bulk}$ intercept ${}^x F$ [at%]	R^2	single cell RSD [†]
<i>P. aeruginosa</i>	2H	0.017 - 0.599	0.30 ± 0.06	0.0 ± 0.0	0.985	12%
<i>S. aureus</i>	2H	0.013 - 0.689	0.34 ± 0.07	0.0 ± 0.0	0.981	18%
<i>P. aeruginosa</i>	${}^{13}C$	1.1 - 10.7	0.17 ± 0.02	0.6 ± 0.0	0.994	1.7%
<i>P. aeruginosa</i>	${}^{15}N$	0.36 - 10.25	0.95 ± 0.04	0.0 ± 0.1	0.999	0.92%
<i>S. aureus</i>	${}^{15}N$	0.36 - 4.50	1.31 ± 0.29	-0.2 ± 0.3	0.981	3.1%

Table C.3: **Calibration parameters for plastic embedded single cell vs. bulk isotope analysis.** Calibration parameters were calculated from $1/x$ weighted linear regression of the average isotopic composition of all single cells for a given standard vs. the measured bulk isotopic composition. Reported errors represent 95% confidence intervals from the regression.

The key observation, however, is the effect of the plastic on the carbon and hydrogen isotopic composition of the microbial isotope standards. As expected, the calibration parameters for both carbon (*P. aeruginosa* only) and hydrogen suggest substantial dilution of the isotopic signal by the plastic polymer, with the slope for carbon dropping from 0.73 ± 0.07 to 0.17 ± 0.02 , and for hydrogen from 0.67 ± 0.05 to 0.30 ± 0.06 (*P. aeruginosa*) and from 0.59 ± 0.05 to 0.31 ± 0.10 (*S. aureus*). To first order, these parameters suggest a dilution of the cellular carbon by $\sim 75\%$ and the cellular hydrogen by $\sim 50\%$. Although the calibration curve for carbon in embedded cells vs. bulk isotopic composition provides a robust linear correlation, the hydrogen calibration curves for both organisms suffer from elevated scatter, likely due to the same effects observed in whole cells (statistical uncertainty in the measurements for each single cell from low ion counts of 2H , as well as random variation in the exact cellular components sampled by the ion beam).

These empirical relationships show that the isotopic enrichment of embedded single cells in both hydrogen and carbon (and of course nitrogen) can be quantified and used to estimate bulk isotopic compositions of individual cells in addition to measuring diversity (which can be assessed in relative terms without calibration). However, our results indicate that the high dilution of C and H by the plastic polymer restrict the accuracy of single cell isotopic measurements at relatively low levels of enrichment, and should not be used for values below $\sim 1000\text{‰}$ (i.e. $2\times$ natural abundance). Additionally, the same caveats as for the analysis of single whole cells (extrapolation to other organisms and morphologies, statistical significance for distinguishing isotopically similar populations, etc.) equally apply. Lastly, given the relatively high scatter for these calibration curves, it is important to apply caution when using them in relating single cell isotopic compositions in plastic back to bulk equivalents.

Supplemental Information D. Effect of isotopic spike present during fixation

In environmental applications of isotope labeling techniques combined with microscopy and imaging mass spectrometry, cells are typically fixed with formaldehyde (or other fixatives) prior to analysis to arrest metabolism and preserve cellular structure. Frequently, fixatives are added to samples still in the presence of (some of) the isotopic label, because extensive washing procedures are either impractical (for very complex samples) or deemed

a risk to the structure and integrity of the target cells. However, fixation can both chemically and/or physically trap unincorporated isotope label that is not actually part of the cell. Such trapped isotope label is retained in excess of true cellular label incorporation, and can lead to an overestimate of microbial activity upon analysis. To estimate the potential extent of this effect, additional aliquots of cells grown without an isotopic label were fixed in the presence of the strongest employed mixture of isotope labels (1% D₂O, 10mM NH₄⁺ with 10% ¹⁵N, 10mM succinate with 10% ¹³C). Table D.4 summarizes the potential effects of the presence of a strong isotopic label during the microbial fixation with formaldehyde prior to embedding in plastic.

Microbe	Isotope	natural abundance cells		spiked during fixation	
		$avg^x F_{cells} [\%]$	$\sigma_{x_F} [\%]$	$avg^x F_{cells} [\%]$	$\sigma_{x_F} [\%]$
PA	¹³ C	0.90	0.06	0.81	0.01
PA	¹⁵ N	0.35	0.01	2.2	0.2
PA	² H	0.021	0.005	0.026	0.005
SA	¹⁵ N	0.361	0.005	2.2	0.1
SA	² H	0.021	0.007	0.026	0.005

Table D.4: **Effect of isotopic spike during fixation.** This table illustrates the effect of the presence of carbon (¹³C succinate), hydrogen (²H₂O) and nitrogen (¹⁵NH₄⁺) isotope labels during culture fixation with formaldehyde on the apparent isotopic composition of the microbial cells. While the presence of ¹³C succinate and ²H₂O does not have a significant enrichment effect within the analytical error, the presence of ¹⁵NH₄ during fixation leads to strong apparent enrichment of the microbial population that can obscure true microbial activity.

The presence of carbon (¹³C succinate) and hydrogen (²H₂O) does not have a significant enrichment effect within the analytical error, but the presence of ¹⁵NH₄ leads to strong apparent enrichment of the microbial population ($^{15}F \approx 2.2\%$, i.e. $\sim 5000\%$ above natural abundance). This is likely a consequence of cross-linking reactions of proteins with the isotope label and subsequent trapping of the label. The effect is considerably exaggerated here due to the nature of the experiment of mixing finely suspended single cells rapidly with both an isotope tracer and a fixating agent. Previous work on environmental samples reported less severe, but still significant abiotic ¹⁵N retention of $^{15}F \approx 0.6\%$ (Orphan et al., 2009). Due to importance of sample conservation, this is often an unavoidable risk when working with a ¹⁵NH₄ label. Ideally, samples are washed to remove the label prior to fixation, but whenever this is not a viable option, it is important to determine the potential extent of this effect in control experiments representative of experimental conditions.

Supplemental Information E. ²H₂O toxicity

Heavy water is known to be toxic at high concentrations (Kushner et al., 1999). We tested the susceptibility of *S. aureus* to ²H₂O by growing it in the medium used throughout this study with varying concentrations of ²H₂O. Two growth experiments with ²H₂O enrichments from 5% to 50% were performed at 37°C in 96 well plates with at least 4 replicates per culture condition. Plates were shaken continuously and optical density (OD_{600nm}) was recorded every 10 minutes. Each experiment was inoculated from an overnight culture that had not previously

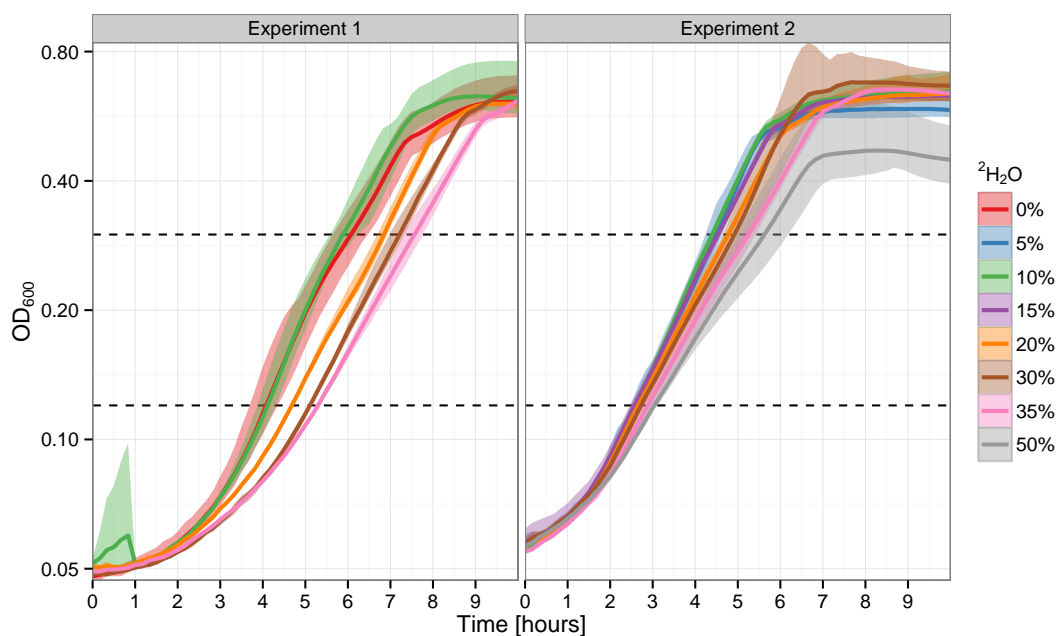


Figure E.9: **Toxicity effects of increasing concentrations of $^2\text{H}_2\text{O}$ on *S. aureus*.** Semi-log growth curves of *S. aureus* in the presence of varying amounts of $^2\text{H}_2\text{O}$ from two separate experiments. Lines represent averages of at least 4 biological replicates, shaded area represents the maximal range of ODs in each condition. Growth rates were evaluated during mid-exponential phase (the optical density interval indicated by the dashed lines).

$^2\text{H}_2\text{O}$	Replicates	Mean Growth rate [1/hr]	Std. Dev.	p-value
0%	8	0.51	0.09	1.00
5%	4	0.48	0.02	0.39
10%	8	0.52	0.03	0.60
15%	4	0.47	0.01	0.27
20%	8	0.43	0.02	0.04
30%	8	0.43	0.04	0.04
35%	8	0.40	0.03	0.01
50%	4	0.36	0.06	0.01

Table E.5: **Changes in growth rates from toxicity effects of increasing concentrations of $^2\text{H}_2\text{O}$.** Summary of the observed growth rates during mid-exponential phase. Reported values are mean growth rates and standard deviation of the biological replicates for each condition. A two sample t-test was used to compare the growth rates for each experimental condition to those of the negative control (0% $^2\text{H}_2\text{O}$). The resulting p-value is reported in the last column.

experienced elevated levels of $^2\text{H}_2\text{O}$.

The results are summarized in Table E.5 and indicate that in this medium, levels of $^2\text{H}_2\text{O}$ exposure above $\sim 15\%$ (i.e., 20%, 30%, 35% and 50%) caused a statistically significant ($p < 0.05$) reduction in the growth rates of *S. aureus*, that is inversely correlated with the intensity of the $^2\text{H}_2\text{O}$ exposure (i.e. the higher the $^2\text{H}_2\text{O}$ concentration, the lower the growth rate). This suggests that isotope labeling experiments with such high levels of $^2\text{H}_2\text{O}$ must be interpreted with caution because the label can affect the growth of *S. aureus*. Throughout this study, we employed labeling concentrations around 0.3%, well below the observed toxicity threshold of 15-20%.

Supplemental Information F. Growth rate calculations

The production and removal of biomass B in continuous culture is determined by the specific growth rate μ (which signifies cellular replication), turnover rate ω (which describes biosynthesis in excess of growth to compensate for degradation and turnover of proteins/lipids), and dilution rate k (which removes biomass from the culturing vessel). The set of differential equations describing the rate of change in total biomass B and the rate of change in new biomass B_{new} is the difference between the synthesis and removal fluxes:

$$\begin{aligned}\frac{dB}{dt} &= (\mu + \omega - \omega - k) \cdot B = (\mu - k) \cdot B \\ \frac{dB_{new}}{dt} &= (\mu + \omega) \cdot B - (k + \omega) \cdot B_{new}\end{aligned}\tag{F.1}$$

A differential equation for the fraction $f_{B_{new}}$ of new vs. total biomass ($f_{B_{new}} = \frac{B_{new}}{B}$) is readily derived using the quotient rule:

$$\begin{aligned}\frac{df_{B_{new}}}{dt} &= \frac{\partial}{\partial t} \left(\frac{B_{new}}{B} \right) = \frac{1}{B} \frac{dB_{new}}{dt} - \frac{B_{new}}{B^2} \frac{dB}{dt} = \frac{1}{B} \left(\frac{dB_{new}}{dt} - f_{B_{new}} \frac{dB}{dt} \right) \\ &= (\mu + \omega) - f_{B_{new}} (k + \omega) - f_{B_{new}} (\mu - k) \\ &= (1 - f_{B_{new}}) \cdot (\mu + \omega)\end{aligned}\tag{F.2}$$

Integration provides a solution for $f_{B_{new}}(t)$ and its derivative $f'_{B_{new}}(t)$:

$$\begin{aligned}f'_{B_{new}}(t) &= (\mu + \omega) \cdot e^{-(\mu + \omega) \cdot t} \\ f_{B_{new}}(t) &= 1 - e^{-(\mu + \omega) \cdot t}\end{aligned}\tag{F.3}$$

Addition of an isotopic label with high fractional abundance F of the rare isotope x to the nutrient pool at time t_0 imparts a distinct isotopic composition ${}^x F_{B_{new}}$ on the newly produced biomass B_{new} . Isotopic mass balance between the new ($f_{B_{new}}$) and old material ($1 - f_{B_{new}}$) determines the overall isotopic composition ${}^x F_B$ of the total biomass. For time-invariant isotopic labels that lead to constant isotopic composition ${}^x F_{B_{new}}$ of all

biomass produced after addition of the isotopic spike, this yields a direct link between isotopic enrichment and growth:

$$\begin{aligned} {}^x F_B(t) &= {}^x F_{B_{new}} \cdot f_{B_{new}}(t) + {}^x F_B(t_0) \cdot (1 - f_{B_{new}}(t)) \\ &= ({}^x F_{B_{new}} - {}^x F_B(t_0)) \cdot \left(1 - e^{-(\mu+\omega) \cdot t}\right) + {}^x F_B(t_0) \end{aligned} \quad (\text{F.4})$$

In continuous culture however, the isotopic spike is slowly diluted out of the system with dilution rate k as new medium replaces isotopically enriched substrate in the chemostat vessel, and the time-dependent isotopic composition of new biomass ${}^x F_{B_{new}}(t)$ has to be taken into consideration:

$${}^x F_B(t) = \left[\int_0^t {}^x F_{B_{new}}(t) \cdot f'_{B_{new}}(t) \cdot dt \right] + {}^x F_B(t_0) \cdot (1 - f_{B_{new}}(t)) \quad (\text{F.5})$$

The exact isotopic composition of new biomass and corresponding solution to equation F.5 depends on the nature of the isotopic label (${}^2\text{H}$ from H_2O / ${}^{15}\text{N}$ from NH_4^+) and is discussed in detail for each label.

${}^2\text{H}$ from H_2O

In this study, the isotopic enrichment of ${}^2\text{H}$ resulting from growth of *S. aureus* in the presence of isotopically spiked water is traced by measuring the isotopic composition of the non-exchangeable hydrogen bound in membrane fatty acids (${}^2F_{fa}$). The isotopic composition of newly synthesized fatty acids (${}^2F_{fa_{new}}$) after administration of the isotopic spike depends (1) on the isotopic composition of the enriched medium water (${}^2F_{water}$) and (2) on the physiology of hydrogen assimilation from water.

(1) The water isotopic composition of the enriched medium is a function of the initial composition of the spiked medium (${}^2F_{spiked}$), and the dilution with fresh medium of original water isotopic composition (${}^2F_{water}(t_0)$) at dilution rate k :

$${}^2F_{water}(t) = {}^2F_{spiked} \cdot e^{-k \cdot t} + {}^2F_{water}(t_0) (1 - e^{-k \cdot t}) \quad (\text{F.6})$$

(2) The isotopic composition of newly synthesized fatty acids can be considered in terms of the combination of the mole fraction of water derived hydrogen x_w and associated net hydrogen isotope fraction $\alpha_{fa/w}$, and substrate derived hydrogen ($x_w - 1$) including metabolic water (Kreuzer-Martin et al., 2006) with average substrate isotopic composition ${}^2F_{sub}$ and associated net isotope fractionation $\alpha_{fa/s}$ (Sessions and Hayes, 2005; Zhang et al., 2009; Valentine, 2009):

$${}^2F_{fa_{new}}(t) = x_w \cdot \alpha_{fa/w} \cdot {}^2F_{water}(t) + (1 - x_w) \cdot \alpha_{fa/s} \cdot {}^2F_{sub} \quad (\text{F.7})$$

For growth in similar medium, the physiological parameters of hydrogen assimilation (x_w , $\alpha_{fa/w}$, $\alpha_{fa/s}$) are assumed to be constant. The appropriate value of the combined water hydrogen assimilation constant

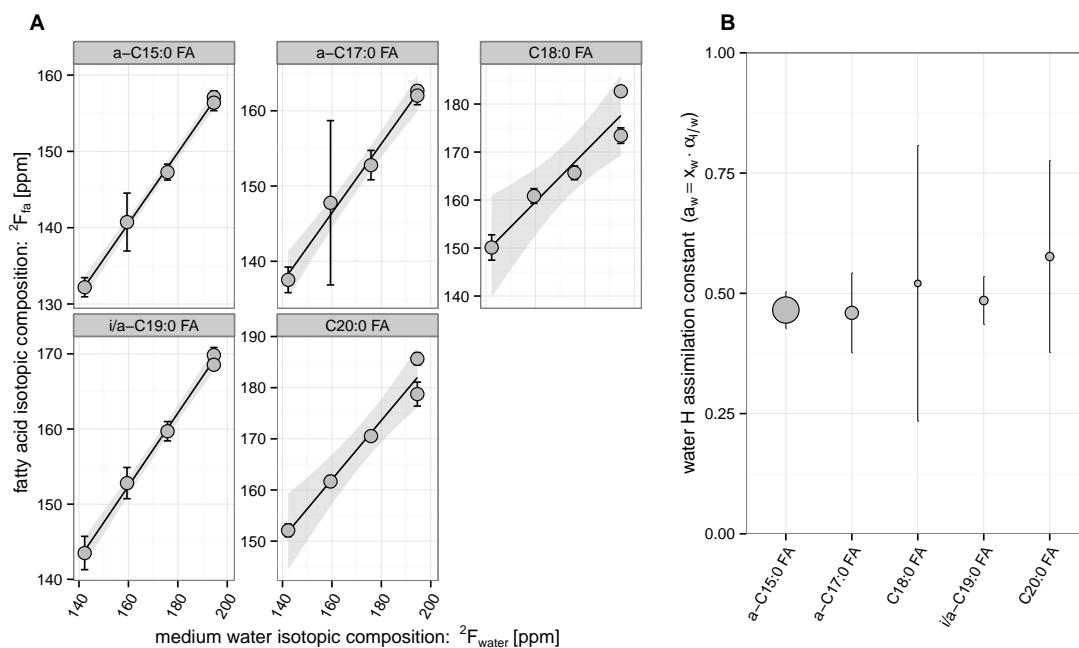


Figure F.10: **Physiological parameters of water hydrogen assimilation for *S. aureus* growing in study medium.** **A:** Regression lines of ${}^2F_{fa}$ vs ${}^2F_{water}$ for individual fatty acids. Error bars on individual data points indicate 95% confidence intervals from up to four analytical replicates. Linear regressions are shown with 95% confidence bands. Some rare fatty acids could not be quantified in all runs. Data points without any error bars are derived from a single analysis. **B:** Summary of the water hydrogen assimilation constants (a_w) derived for individual fatty acids from regression analysis of A. Size of symbols indicates the relative membrane abundance of the individual fatty acids. Error bars indicate 95% confidence intervals of the coefficients from the linear regression fit.

Compound	% Membrane	water H assimilation constant (a_w)	R^2
a-C15:0 FA	46.7	0.47 ± 0.04	0.998
a-C17:0 FA	20.2	0.46 ± 0.08	0.990
C18:0 FA	6.7	0.52 ± 0.29	0.918
i/a-C19:0 FA	10.7	0.49 ± 0.05	0.997
C20:0 FA	10.1	0.58 ± 0.20	0.966

Table F.6: **Water hydrogen assimilation constants for *S. aureus* growing in study medium.** Summary of the water hydrogen assimilation constants (a_w) of all major fatty acids (>5% relative abundance). Errors represent 95% confidence intervals of the coefficients from the linear regression fit.

$a_w = x_w \cdot \alpha_{fa/w}$ for *S. aureus* growing in the medium used in this study was determined following the approach of Zhang et al. (2009). Briefly, *S. aureus* was grown in batch culture experiments with four different water isotopic compositions and a_w was determined for all major membrane fatty acids from the slopes of ${}^2F_{fa}$ vs. ${}^2F_{water}$ (Figure F.10 and Table F.6). For calculations involving bulk fatty acid hydrogen isotope compositions, an average value for a_w (average $a_w = 0.48$) was determined from all fatty acids' a_w -values weighted by the relative abundances of the individual fatty acids. The ${}^2F_{sub}$ -dependent contribution to fatty acid hydrogen $((1 - x_w) \cdot$

$\alpha_{fa/s} \cdot {}^2F_{sub}$) was determined from a_w and the water and fatty acid isotopic compositions in each continuous culture experiment prior to the addition of isotope tracers ($(1 - x_w) \cdot \alpha_{fa/s} \cdot {}^2F_{sub} = {}^2F_{fa}(t_0) - a_w \cdot {}^2F_{water}(t_0)$). Equation F.7 thus becomes:

$$\begin{aligned} {}^2F_{fa_{new}}(t) &= a_w \cdot ({}^2F_{water}(t) - {}^2F_{water}(t_0)) + {}^2F_{fa}(t_0) \\ &= a_w \cdot ({}^2F_{spiked} - {}^2F_{water}(t_0)) \cdot e^{-k \cdot t} + {}^2F_{fa}(t_0) \end{aligned} \quad (F.8)$$

Substitution into equation F.5 finally yields the following solution, which is simplified by replacing the biosynthetic rates μ (cellular replication) and ω_{fa} (turnover; here for fatty acids) with the combined total growth activity rate $\mu_{act} = \mu + \omega_{fa}$ representing the overall rate of biosynthesis:

$$\begin{aligned} {}^2F_{fa}(t) &= \int_0^t {}^2F_{fa_{new}}(t) \cdot f'_{B_{new}}(t) \cdot dt + {}^2F_{fa}(t_0) \cdot (1 - f_{B_{new}}(t)) \\ &= \int_0^t a_w \cdot ({}^2F_{spiked} - {}^2F_{water}(t_0)) \cdot \mu_{act} \cdot e^{-(\mu_{act}+k) \cdot t} \cdot dt \\ &\quad + \int_0^t {}^2F_{fa}(t_0) \cdot \mu_{act} \cdot e^{-\mu_{act} \cdot t} \cdot dt + {}^2F_{fa}(t_0) \cdot e^{-\mu_{act} \cdot t} \\ &= a_w \cdot ({}^2F_{spiked} - {}^2F_{water}(t_0)) \cdot \frac{\mu_{act}}{\mu_{act} + k} \cdot (1 - e^{-(\mu_{act}+k) \cdot t}) + {}^2F_{fa}(t_0) \end{aligned} \quad (F.9)$$

In continuous culture at steady state, the dilution rate k sets the average growth rate of the population ($\frac{dB}{dt} = 0 \Rightarrow \bar{\mu} = k$). Here, using equation F.9, the growth activity rate μ_{act} was calculated on a *single cell* basis from NanoSIMS hydrogen isotope measurements. For each continuous culture experiment, the dilution rate k was set by the experimental setup, water isotopic compositions ${}^2F_{spiked}$ and ${}^2F_{water}(t_0)$ were measured as described in the Experimental Procedures, and bulk membrane fatty acid isotopic compositions ${}^2F_{fa}(t)$ and ${}^2F_{fa}(t_0)$ were determined from single cell hydrogen isotope measurements using the calibrations discussed in the main text.

¹⁵N from NH₄⁺

The isotopic enrichment of ¹⁵N resulting from growth of *S. aureus* in the presence of isotopically spiked ammonium is traced by measuring the bulk nitrogen isotopic composition (${}^{15}F_{bulk}$) of single cells. Like ²H from H₂O, the isotopic composition of newly synthesized biomass (${}^{15}F_{new}$) after administration of the isotopic spike depends (1) on the isotopic composition of the enriched ammonium (${}^{15}F_{NH_4^+}$) and (2) on the physiology of nitrogen assimilation.

(1) The nitrogen isotopic composition of the enriched ammonium in the medium is a function of the initial concentration and composition of ammonium in the spiked medium ($[NH_4^+]_{spiked}$ and ${}^{15}F_{spiked}$), and the dilution with fresh medium back towards the steady-state equilibrium concentration ($[NH_4^+]_{eq}$) and natural isotopic

composition ($^{15}F_{nat}$) at dilution rate k :

$$^{15}F_{NH_4^+}(t) = \frac{[NH_4^+]_{spiked} \cdot ^{15}F_{spiked} \cdot e^{-k \cdot t} + [NH_4^+]_{eq} \cdot ^{15}F_{nat} \cdot (1 - e^{-k \cdot t})}{[NH_4^+]_{spiked} \cdot e^{-k \cdot t} + [NH_4^+]_{eq} \cdot (1 - e^{-k \cdot t})} \quad (F.10)$$

(2) The nitrogen isotope composition of newly synthesized biomass ($^{15}F_{new}$) depends on the relative contribution of cellular nitrogen assimilated from ammonium ($x_{NH_4^+}$) vs. all other nitrogen sources ($1 - x_{NH_4^+}$). It is important to note that it does not matter whether the steady-state pool of ammonium present at the time of spiking is composed only of the initial pool of ammonium added to the medium, or whether it contains any additional ammonium released by potential spontaneous decomposition of amino acids, assuming that both sources reflect a natural abundance isotope composition ($^{15}F_{nat}$). All nitrogen assimilated from the ammonium pool after addition of the isotopically enriched spike is isotopically distinct with composition $^{15}F_{NH_4^+}(t)$ whereas nitrogen assimilated from all other nitrogen sources (amino acids present in the culture medium) continues to reflect a natural abundance isotope composition ($^{15}F_{nat}$). The isotopic composition of cellular nitrogen derived from all natural abundance materials (unlabeled ammonium and amino acids) is assumed to be invariant and reflected in the cellular nitrogen isotope value prior to isotope labeling ($^{15}F_{bulk}(t_0) = ^{15}F_{nat}$). Isotope fractionation associated with nitrogen assimilation from ammonium is assumed to be negligible ($^{15}\alpha \approx 1$) in the context of isotope labeling with highly enriched ^{15}N .

$$^{15}F_{new}(t) = x_{NH_4^+} \cdot ^{15}F_{NH_4^+}(t) + (1 - x_{NH_4^+}) \cdot ^{15}F_{bulk}(t_0) \quad (F.11)$$

Substituting equations F.10 and F.11 into equation F.5 yields:

$$\begin{aligned} ^{15}F_{bulk}(t) &= \int_0^t ^{15}F_{new}(t) \cdot f'_{B_{new}}(t) \cdot dt + ^{15}F_{bulk}(t_0) \cdot (1 - f_{B_{new}}(t)) \\ &= x_{NH_4^+} \cdot \int_0^t \left(^{15}F_{NH_4^+}(t) - ^{15}F_{bulk}(t_0) \right) \cdot (\mu + \omega_N) \cdot e^{-(\mu + \omega_N) \cdot t} \cdot dt \\ &\quad + \int_0^t ^{15}F_{bulk}(t_0) \cdot (\mu + \omega_N) \cdot e^{-(\mu + \omega_N) \cdot t} \cdot dt + ^{15}F_{bulk}(t_0) \cdot e^{-(\mu + \omega_N) \cdot t} \\ &= x_{NH_4^+} \cdot \int_0^t \left(\frac{[NH_4^+]_{spiked} \cdot ^{15}F_{spiked} + [NH_4^+]_{eq} \cdot ^{15}F_{bulk}(t_0) \cdot (e^{k \cdot t} - 1)}{[NH_4^+]_{spiked} + [NH_4^+]_{eq} \cdot (e^{k \cdot t} - 1)} - \right. \\ &\quad \left. - ^{15}F_{bulk}(t_0) \right) \cdot (\mu + \omega_N) \cdot e^{-(\mu + \omega_N) \cdot t} \cdot dt + ^{15}F_{bulk}(t_0) \end{aligned} \quad (F.12)$$

For each continuous culture experiment, the fraction of nitrogen assimilated from ammonium $x_{NH_4^+}$ was estimated on a single cell basis by numerical integration of equation F.12 with k set by the experimental setup and single cell growth rates derived from corresponding hydrogen isotope measurements (equation F.9). It is important to note that hydrogen derived growth rates μ_{act} include a component of fatty acid turnover ω_{fa}

that is unlikely to be representative of cellular nitrogen turnover ω_N . To account for this difference, hydrogen derived measurements of μ_{act} were scaled to the known average growth rate in each experiment ($\bar{\mu} = k$) to provide estimates of single cell μ , and nitrogen turnover was estimated from prior work on protein turnover ($\omega_N = 0.0275 \text{ hr}^{-1}$, Pine (1970, 1972)) as discussed in the text. Ammonium concentrations $[\text{NH}_4^+]_{spiked}$ and $[\text{NH}_4^+]_{eq}$ were measured as described in the Experimental Procedures, and the isotopic compositions $^{15}\text{F}_{bulk}(t)$ and $^{15}\text{F}_{bulk}(t_0)$ were calculated from single cell nitrogen isotope measurements.

Supplemental Information G. Incubation time requirements

The incubation time requirements illustrated in Figure 1 are estimated for a given heavy water isotopic spike $^2\text{F}_{spiked}$ and population generation time T as follows. Assuming that the isotopic label is not diluted out of the system ($k = 0$), Equation F.9 simplifies to

$$^2\text{F}_{fa}(t) = a_w \cdot (^2\text{F}_{spiked} - ^2\text{F}_{water}(t_0)) \cdot (1 - e^{-\mu \cdot t}) + ^2\text{F}_{fa}(t_0) \quad (\text{G.1})$$

Substituting the generation time for the growth rate ($\mu = \frac{\ln 2}{T}$), and solving for the time t_{label} required to reach a final isotopic enrichment of $^2\text{F}_{fa}(t_{label}) = ^2\text{F}_{final}$ yields

$$t_{label} = \frac{T}{\ln 2} \cdot \ln \left(\frac{a_w \cdot (^2\text{F}_{spiked} - ^2\text{F}_{water}(t_0))}{a_w \cdot (^2\text{F}_{spiked} - ^2\text{F}_{water}(t_0)) - (^2\text{F}_{final} - ^2\text{F}_{fa}(t_0))} \right) \quad (\text{G.2})$$

with water and fatty acid isotopic compositions before spiking (at t_0) approximated by natural abundance hydrogen isotope values ($^2\text{F}_{water}(t_0) = ^2\text{F}_{fa}(t_0) = ^2\text{F}_{nat} = 0.015574 \text{ at}\%$). For the purpose of this minimum incubation time estimate, the water hydrogen assimilation constant a_w was set to 0.49, a conservative estimate based on the average values of a_w measured for complex media in this study and in Zhang and Rock (2008). Higher values of a_w , such as those measured for heterotrophic growth conditions with TCA cycle intermediates as sole carbon sources, and for autotrophic metabolisms (e.g., Zhang and Rock, 2008), would always lead to *shorter* incubation time requirements.

Supplemental Information H. Log-normal growth rate distribution

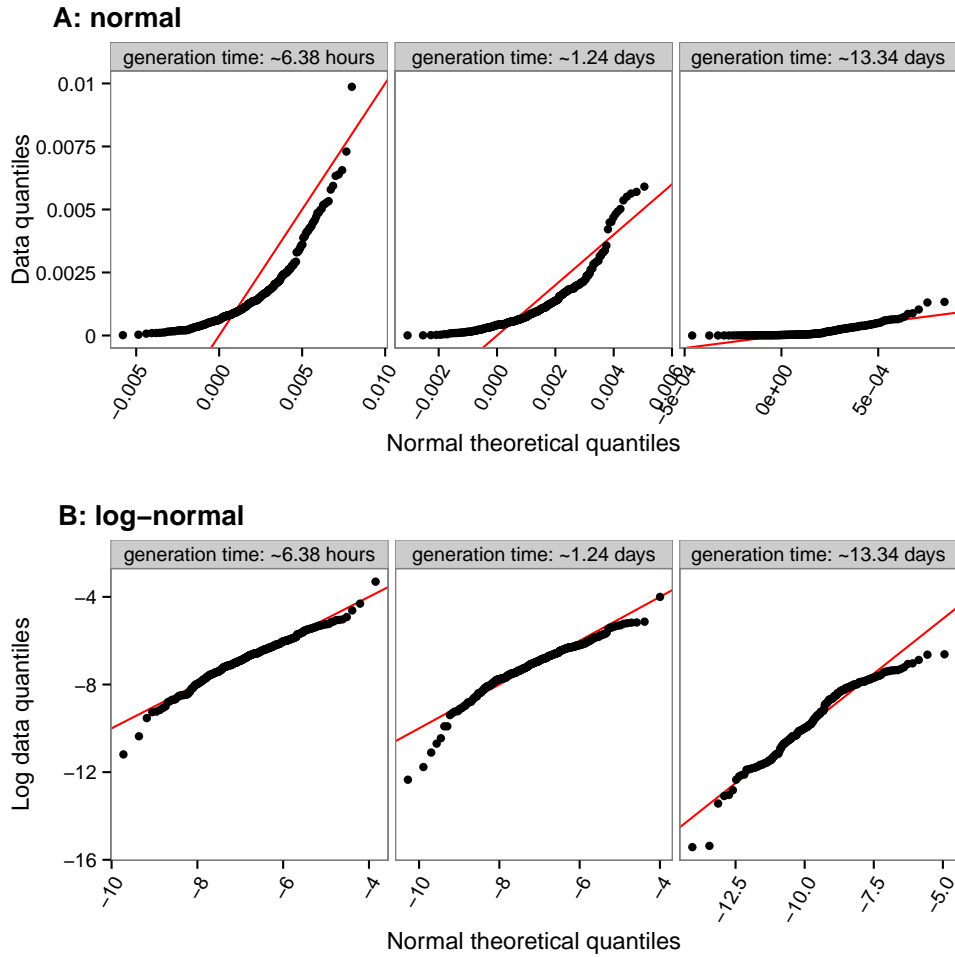


Figure H.11: **Single cell growth rates fit log-normal distribution.** Quantile plots of the measured single cell growth rates vs. theoretical distributions show that the data is described more accurately by a log-normal (**B**) rather than a normal distribution (**A**).

Supplemental Information I. Additional data tables and figures

Organism	$^2\text{H } F_{fa}$ [%]	$^{15}\text{N } F_{bulk}$ [%]	$^{13}\text{C } F_{bulk}$ [%]
<i>P. aeruginosa</i>	0.017 ± 0.000	0.360 ± 0.003	1.084 ± 0.001
<i>P. aeruginosa</i>	0.030 ± 0.001	0.378 ± 0.002	1.198 ± 0.007
<i>P. aeruginosa</i>	0.177 ± 0.006	1.485 ± 0.007	1.646 ± 0.001
<i>P. aeruginosa</i>	0.237 ± 0.006	3.828 ± 0.044	2.152 ± 0.007
<i>P. aeruginosa</i>	0.599 ± 0.042	10.247 ± 0.120	10.657 ± 0.102
<i>S. aureus</i>	0.013 ± 0.000	0.364 ± 0.005	
<i>S. aureus</i>	0.026 ± 0.000	0.369 ± 0.004	
<i>S. aureus</i>	0.080 ± 0.002	0.860 ± 0.029	
<i>S. aureus</i>	0.276 ± 0.011	0.959 ± 0.001	
<i>S. aureus</i>	0.689 ± 0.056	4.496 ± 0.098	

Table I.7: **Bulk isotopic composition of microbial NanoSIMS standards.** Standards are from single pure cultures harvested in mid-exponential phase. Reported bulk hydrogen isotope compositions represent the mass balance weighted average isotopic composition of the whole membrane from all major fatty acid components. Reported errors represent 95% confidence intervals from replicate analyses.

Continuous culture generation time	Time after addition of isotopic spike	$^2\text{H } F_{fa}$ [%]
6.38 hours	0 seconds	0.0133 ± 0.0009
6.38 hours	10 minutes	0.0152 ± 0.0003
6.38 hours	20 minutes	0.0174 ± 0.0010
6.38 hours	30 minutes	0.0191 ± 0.0003
6.38 hours	40 minutes	0.0207 ± 0.0008
6.38 hours	50 minutes	0.0231 ± 0.0020
6.38 hours	1 hours	0.0250 ± 0.0019
1.24 days	0 seconds	0.0143 ± 0.0002
1.24 days	40 minutes	0.0160 ± 0.0004
1.24 days	1.37 hours	0.0182 ± 0.0004
1.24 days	2 hours	0.0199 ± 0.0004
1.24 days	2.67 hours	0.0222 ± 0.0008
1.24 days	3.33 hours	0.0239 ± 0.0012
13.34 days	0 seconds	0.0144 ± 0.0002
13.34 days	5 hours	0.0166 ± 0.0002
13.34 days	10 hours	0.0191 ± 0.0004
13.34 days	15 hours	0.0215 ± 0.0006
13.34 days	20 hours	0.0239 ± 0.0009
13.34 days	1.04 days	0.0268 ± 0.0010
13.34 days	1.25 days	0.0303 ± 0.0012

Table I.8: **Bulk isotopic composition of isotopically labeled cells in continuous culture.** Reported bulk hydrogen isotope compositions represent the mass balance weighted average isotopic composition of the whole membrane from all major fatty acid components. Reported errors represent 95% confidence intervals from replicate analyses.

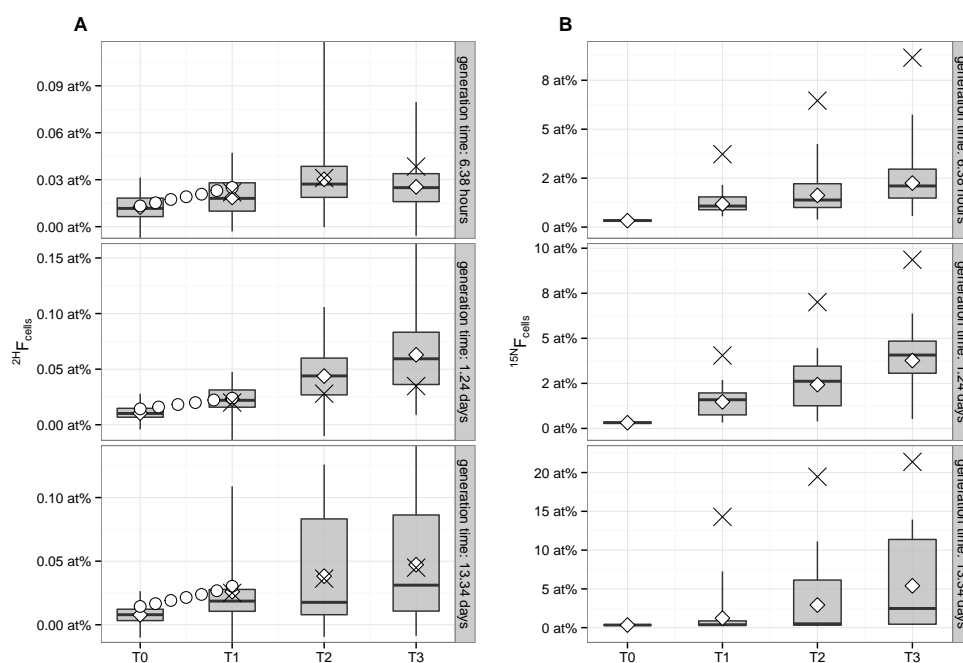


Figure I.12: **Single cell isotopic compositions.** The three panels show the single cell data from continuous culture experiments at different growth rates. All single cell data is corrected to reflect the corresponding bulk fatty acid composition for ^2H (A) and bulk cell composition for ^{15}N (B) using the calibrations described in the text. The gray bands for each time point represent the range that comprises 50% of the single cell data. The whiskers represent the entire range of all single cells (upper and lower quartile). White diamonds represent the average isotopic composition of all measured single cells at a time point, and the black lines represent the median. Differences between the mean and the median reflect a skewed distribution in the isotopic composition of individual cells that is discussed in detail in the text. The white circles show the bulk membrane fatty acid hydrogen isotopic compositions (data from Table I.8). The crosses represent the theoretically expected average isotopic composition at each time point, assuming no fatty acid turnover (^2H enrichment in A), and nitrogen turnover on the order of $\omega_N=2.75\%/hr$ (as discussed in the text) with ammonium as the only source of nitrogen used by the cells (^{15}N enrichment in B). The substantial overestimate of the theoretical prediction for ^{15}N enrichment highlights the importance of alternative, unlabelled nitrogen sources for the cells (here, amino acids supplied in the medium), as discussed in the text.